Mutational Analysis of the Nuclease Domain of *Escherichia coli* Ribonuclease III. Identification of Conserved Acidic Residues that Are Important for Catalytic Function *in Vitro*†

Weimei Sun,‡,§ Gang Li,‡,|| and Allen W. Nicholson*

Department of Chemistry and Center for Biotechnology, Temple University, Philadelphia, Pennsylvania 19122

Received April 14, 2004; Revised Manuscript Received July 11, 2004

ABSTRACT: The ribonuclease III superfamily represents a structurally distinct group of double-strand-specific endonucleases with essential roles in RNA maturation, RNA decay, and gene silencing. Bacterial RNase III orthologs exhibit the simplest structures, with an N-terminal nuclease domain and a C-terminal double-stranded RNA-binding domain (dsRBD), and are active as homodimers. The nuclease domain contains conserved acidic amino acids, which in *Escherichia coli* RNase III are E38, E41, D45, E65, E100, D114, and E117. On the basis of a previously reported crystal structure of the nuclease domain of *Aquifex aeolicus* RNase III, the E41, D114, and E117 side chains of *E. coli* RNase III are expected to be coordinated to a divalent metal ion (Mg^{2+} or Mn^{2+}). It is shown here that the RNase III[E41A] and RNase III[D114A] mutants exhibit catalytic activities *in vitro* in 10 mM Mg^{2+} buffer that are comparable to that of the wild-type enzyme. However, at 1 mM Mg^{2+}, the activities are significantly lower, which suggests a weakened affinity for metal. While RNase III[E41A] and RNase III[D114A] have K^{Mg} values that are ∼2.8-fold larger than the K^{Mg} of RNase III (0.46 mM), the RNase III[E41A/D114A] double mutant has a K^{Mg} of 39 mM, suggesting a redundant function for the two side chains. RNase III[E38A], RNase III[E65A], and RNase III[E100A] also require higher Mg^{2+} concentrations for optimal activity, with RNase III[E100A] exhibiting the largest K^{Mg}. RNase III[D45A], RNase III[D45E], and RNase III[D45N] exhibit negligible activities, regardless of the Mg^{2+} concentration, indicating a stringent functional requirement for an aspartate side chain. RNase III[D45E] activity is partially rescued by Mn^{2+}. The potential functions of the conserved acidic residues are discussed in the context of the crystallographic data and proposed catalytic mechanisms.

The enzymatic cleavage of double-stranded (ds) RNA is an obligatory step in the maturation and decay of many coding and noncoding RNAs in eukaryotic and prokaryotic cells. The processing of dsRNA[1] also is a required step in RNA interference and related RNA-dependent gene silencing mechanisms (*1*, *2*). The primary agents of dsRNA cleavage belong to the highly conserved and structurally distinct ribonuclease III superfamily (*1*−*3*). Studies on *Escherichia coli* RNase III (*4*) have provided useful insight into a conserved mechanism of dsRNA processing, and also have revealed an essential involvement of RNase III in bacterial RNA metabolism and gene regulation (*1*, *3*−*5*). *E. coli* RNase III can function as a maturation nuclease, cleaving precursors to rRNAs, tRNAs, and mRNAs either to create the mature species directly or to provide intermediates that undergo subsequent processing events (*3*, *5*). *E. coli* RNase III also participates in RNA degradation pathways. For example, RNase III cleavage of a double-helical element within the 5′-untranslated region of its own mRNA promotes the rapid destruction of the RNA, providing negative autocontrol (*6*, *7*). RNase III participates in gene regulation by cleaving duplex structures created by antisense RNA binding to the target RNA sequence (*8*). In most if not all of these reactions, the RNAs undergo site-specific cleavage, with the target phosphodiester(s) identified by a combination of substrate sequence and structural elements (*1*, *3*, *5*).

RNase III superfamily members are characterized by conserved structural domains. Bacterial RNase III orthologs possess the simplest structures, with the ∼230-amino acid polypeptide containing an N-terminal nuclease domain and a C-terminal dsRNA-binding domain (dsRBD), the latter being defined by the presence of the conserved dsRNA-binding motif (dsRBM) (*9*, *10*) (Figure 1A). The dsRBD is important for *E. coli* RNase III activity *in vivo* and in standard reaction conditions *in vitro* (*11*). However, a truncated form of *E. coli* RNase III containing only the nuclease domain can cleave the substrate in the presence of low salt and Mn^{2+}, and retains double-strand specificity (*12*).

† Research supported by NIH Grant GM56457.

* To whom correspondence should be addressed: Department of Chemistry, Temple University, 1901 N. 13th St., Philadelphia, PA 19122. Phone: (215) 204-4410. Fax: (215) 204-1532. E-mail: anichol@temple.edu.

‡ These authors contributed equally to this project.

§ Present address: Lexicon Genetics, 8800 Technology Forest Place, The Woodlands, TX 77381.

|| Present address: Wayne State University School of Medicine, 540 E. Canfield, Detroit, MI 48201.

[1] Abbreviations: dsRBD, double-stranded RNA-binding domain; dsRNA, double-stranded RNA; DTT, dithiothreitol; EDTA, ethylenediaminetetraacetic acid; IPTG, isopropyl β-D-thiogalactopyranoside; nt, nucleotide; RNase, ribonuclease; SDS−PAGE, sodium dodecyl sulfate−polyacrylamide gel electrophoresis; WT, wild-type.

10.1021/bi049258i CCC: $27.50
Published on Web 09/25/2004

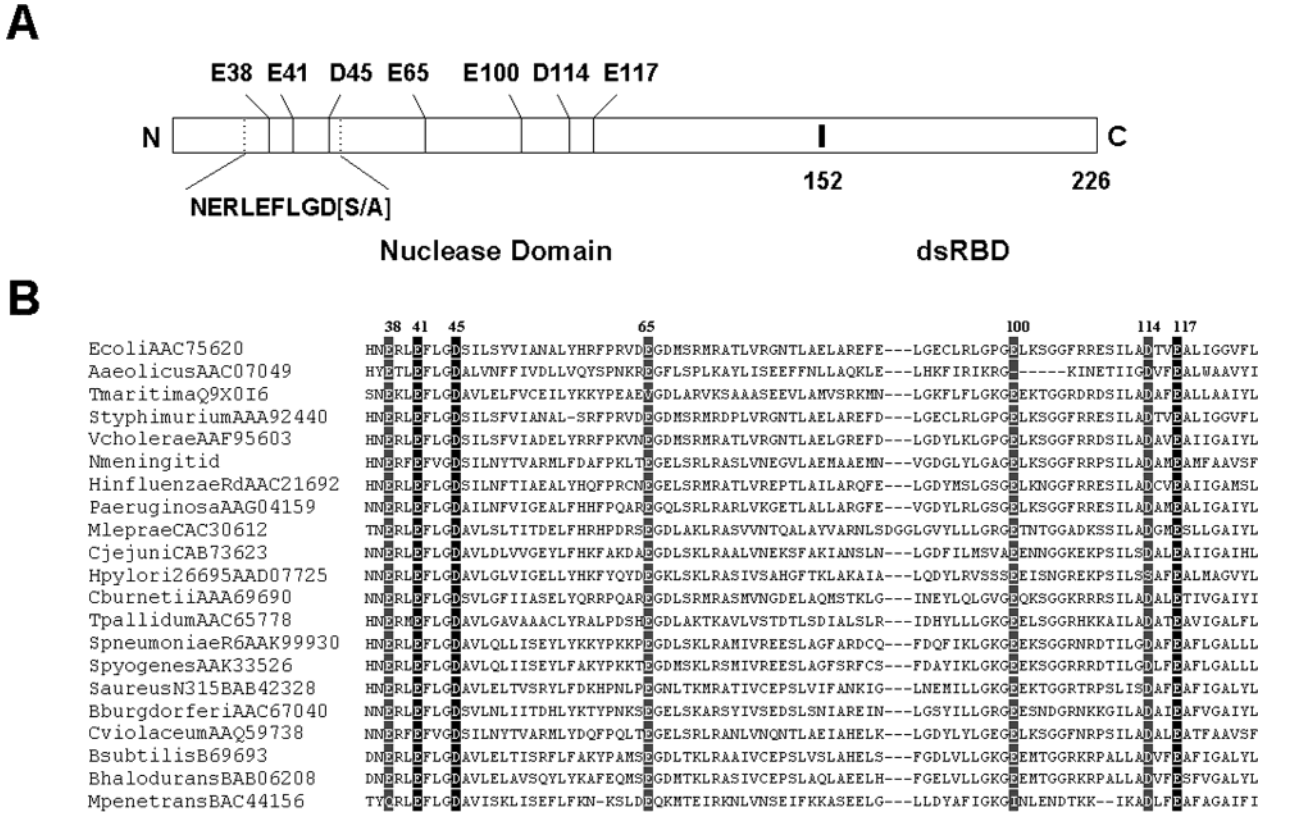

FIGURE 1: Domain structure and conserved amino acids in bacterial ribonuclease III. (A) Domain structure. Residue numbers refer to the *E. coli* RNase III polypeptide. The conserved acidic residues analyzed in this study are given above the diagram. (B) Sequence alignment of nuclease domains. For convenience, the alignment does not include sequences that are N-terminal to the signature sequence (NERLEFLGD-[S/A]). Thus, for *E. coli* RNase III, the first residue shown is H36. Highly conserved acidic side chains are indicated by reverse highlighting, with the apparent invariant residues highlighted in black. Several sequence deviations relevant to this study were noted: (i) E → V at position 65 in *T. maritima* RNase III, (ii) a six-amino acid deletion that includes residue 100 in *A. aeolicus* RNase III, and (iii) E → Q at position 38 and E → I at position 100 in *M. penetrans* RNase III and D → S at position 114 in *H. pylori* RNase III (*E. coli* RNase III numbering system used). We have verified the sequences of the *T. maritima* and *A. aeolicus* RNase III genes, and also found that both proteins in purified form are catalytically active *in vitro* (W. Meng and A. W. Nicholson, unpublished results). Since only a single nucleotide change would be required for the E38Q difference in *M. penetrans* RNase III, a sequencing error cannot be ruled out. For the E100I difference, two nucleotide changes would be necessary, so it is reasonable to assume that this substitution is real. In *H. pylori* RNase III, the D114S difference also would entail two nucleotide changes.

A crystallographic analysis of the nuclease domain of *Aquifex aeolicus* RNase III reveals a homodimeric structure that exhibits a novel all-α fold (*13*). The subunit interface is proposed to provide the dsRNA binding site (*13*).

The mechanism of cleavage of dsRNA by RNase III is only partly understood, but a growing body of biochemical and structural data indicates that the mechanism is common to all superfamily members. For every RNase III ortholog so far examined, target site phosphodiesters are hydrolyzed to provide 5′-phosphate, 3′-hydroxyl product termini. The cleavage reaction is dependent on a divalent metal ion, with Mg^{2+} as the preferred species (*1*, *5*, *14*). Enzyme kinetic studies indicate that the reaction nucleophile is a metal-bound hydroxide (*15*). The homodimeric nuclease domain of *A. aeolicus* RNase III contains two metal binding sites at opposite ends of the subunit interface (*13*). The sites include the side chains of several acidic residues, which in *E. coli* RNase III are E38, E41, D45, E65, D114, and E117. Sequence alignment (Figure 1B) indicates a strong conservation of these residues among bacterial RNase III orthologs. Three of the residues (E41, D114, and E117) interact with a metal ion (Figure 2), and are expected to be important for activity by providing a binding site for the required metal cofactor. In fact, conversion of E117 to alanine virtually abolishes *E. coli* RNase III activity *in vitro* (*16*), and the E117D, E117Q, and E117K mutations, also expected to disrupt metal binding, are catalytically defective (*16*−*18*). The functional contributions of the other conserved acidic residues, including E100, which is not adjacent to the metal binding site, have not been assessed. We present here a biochemical analysis of *E. coli* RNase III mutants with alanine substitutions of conserved acidic residues in the nuclease domain.

EXPERIMENTAL PROCEDURES

Materials. Water was deionized and distilled. Chemicals and reagents were molecular biology grade and were purchased from Sigma or Fisher Scientific. Standardized 1 M solutions of $MgCl_2$ and $MnCl_2$ were obtained from Sigma. Nonradioactive ribonucleoside 5′-triphosphates were obtained from Amersham-Pharmacia Biotech, while [γ-^{32}P]ATP (3000 Ci/mmol), [α-^{32}P]UTP (3000 Ci/mmol), and [α-^{32}P]CTP (3000 Ci/mmol) were purchased from Perkin-Elmer. Restriction enzymes, Vent DNA polymerase, and T4 polynucleotide kinase were obtained from New England Biolabs. Calf intestine alkaline phosphatase was obtained from Roche Molecular Biosciences. T7 RNA polymerase was purified in-house as described previously (*19*). Oligodeoxynucleotides used for PCR mutagenesis or in transcription reactions (see

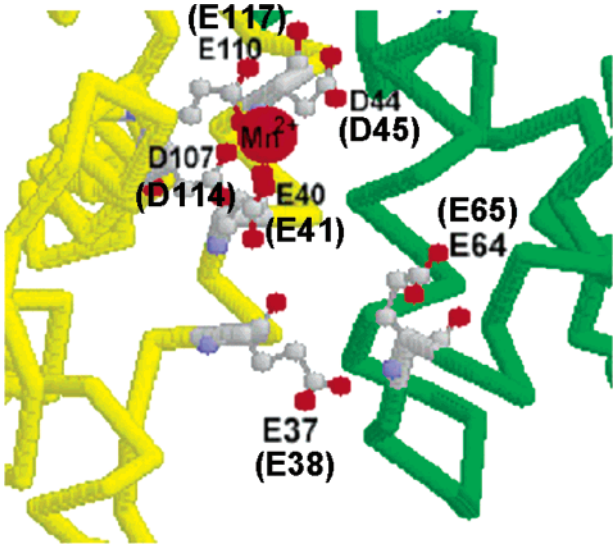

FIGURE 2: Positions of conserved acidic amino acids and the divalent metal ion binding site in the homodimeric nuclease domain of *A. aeolicus* RNase III. The structure is based on an X-ray diffraction study (*13*) and shows the positions of the residues that correspond to E38, E41, D45, E65, D114, and E117 of *E. coli* RNase III (residue numbers given in parentheses). The Mn^{2+} ion is represented by the solid red sphere.

below) were obtained in deprotected form from Invitrogen, and were further purified by denaturing gel electrophoresis (*20*).

Construction, Overproduction, and Purification of RNase III Alanine Mutants. E. coli RNase III mutants were purified in an N-terminally His_6-tagged form (*20*). Construction of the RNase III mutant genes used a two-step PCR procedure as previously described (*16*, *18*). Briefly, the pET-15b(rnc) plasmid template contained the *E. coli* RNase III (*rnc*) gene cloned between the *Nde*I and *Bam*HI sites. First-step PCR employed Vent DNA polymerase and the mutagenic oligonucleotide paired with either the *rnc* gene 5′-end primer or 3′-end primer, as appropriate (oligonucleotide sequences are available upon request). Second-step PCR used the gel-purified product of the first reaction paired with the *rnc* 5′-end primer or 3′-end primer, as appropriate, to generate the full-length mutant gene. The gel-purified product was cloned into the *Nde*I and *Bam*HI sites of pET-15b, and recombinant plasmids were isolated from *E. coli* DH10B cells (Invitrogen) that were electroporated with aliquots of ligation reaction mixtures. Mutations were verified by DNA sequencing. To overproduce the protein, the recombinant plasmids were introduced into *E. coli* BL21(DE3)*rnc105*, *recA* cells (*20*). The *recA* allele served to suppress recombination between host and plasmid sequences. The *rnc105* allele (G44D) (*21*, *22*) abolished the activity of the chromosomally encoded RNase III, which otherwise could compromise the analysis of RNase III mutants with low-level activities (*20*). RNase III mutant overproduction was induced by IPTG treatment of mid-log bacterial cultures grown in LB with ampicillin at 37 °C (*20*). Following further growth with aeration for 4 h at 37 °C, cells were collected by centrifugation and stored at −20 °C prior to further use. To ensure that the desired RNase III mutant was overproduced, the plasmid was purified from an aliquot of the cell culture and the *rnc* gene was sequenced. Protein was purified as described previously (*20*) from the soluble portion of sonicated cell extracts using Ni^{2+} affinity chromatography (His-Bind resin, Novagen). SDS−PAGE analysis indicated a protein purity of at least 90%, and the preparation was free of any adventitious ribonucleolytic activity. Proteins were stored at −20 °C in buffer [30 mM Tris-HCl (pH 7.9), 500 mM NaCl, 0.5 mM DTT, and 0.5 mM EDTA] containing 50% glycerol. Protein concentrations did not appreciably change under these conditions. The N-terminal His_6 tag was not removed, as it has a negligible effect on RNase III activity (*20*). For convenience, His_6-RNase III [or His_6-RNase III mutant] is termed RNase III (or specific RNase III mutant).

Substrate Cleavage Assay. R1.1 RNA (Figure 3A) was synthesized in internally ^{32}P-labeled form as described previously (*20*), by transcription of an oligodeoxynucleotide template using T7 RNA polymerase and in the presence of either [α-^{32}P]CTP or [α-^{32}P]UTP (final specific activity of 100 Ci/mol). R1.1 RNA (5′-^{32}P-labeled) was obtained by treatment of dephosphorylated (nonradioactive) R1.1 RNA with T4 polynucleotide kinase and [γ-^{32}P]ATP (3000 Ci/mmol) (*20*). Radiolabeled R1.1 RNA was purified by gel electrophoresis and stored at −20 °C in 10 mM Tris-HCl (pH 7.5) and 1 mM EDTA. Cleavage assays were carried out essentially as described previously (*20*), with substrate treated to a heating−snap cooling step prior to use. Cleavage assay buffer consisted of 200 mM NaCl, 30 mM Tris-HCl (pH 7.5), 0.1 mM EDTA, and divalent metal ion as indicated. Assays involved incubation of RNA with enzyme for 5 min at 37 °C, and the reaction was initiated by adding the divalent metal ion as indicated. Reaction mixtures were incubated at 37 °C for the indicated times, and then reactions were stopped by adding EDTA (final concentration of 20 mM). Additional aspects of the cleavage assays, including the RNase III concentrations, are given in the appropriate figure legends or table footnotes. Reactions were analyzed by electrophoresis on a 12% polyacrylamide gel containing 7 M urea. Reactions were visualized by phosphorimaging (Typhoon 9400 System, Amersham Biosciences) and quantitated using ImageQuant (*12*, *18*, *20*). Kinetic analyses and curve fitting were carried out using Kaleidagraph (version 3.5).

Substrate Binding Assay. Gel mobility shift assays were carried out essentially as described previously (*20*). Briefly, 5′-^{32}P-labeled R1.1 RNA (3000 Ci/mmol) was incubated with RNase III in binding buffer (*20*) supplemented with 5 mM $CaCl_2$. Aliquots of the reactions were electrophoresed at ∼5 °C in a 6% polyacrylamide gel containing TBE buffer, also supplemented with 5 mM $CaCl_2$. Binding reactions were visualized by phosphorimaging (*20*). The apparent dissociation constants (K'_D values) of the R1.1 RNA−RNase III complexes were determined as described previously (*18*, *20*).

RESULTS

Catalytic Activities of the RNase III[E41A] and RNase III[D114A] Mutants. The *A. aeolicus* RNase III E40 and D107 side chains (corresponding to those of E41 and D114, respectively, in *E. coli* RNase III) interact with a divalent metal ion (*13*) (Figure 2). To assess the side chain requirements for activity, E41 and D114 were separately changed to alanine. The mutant proteins were able to be overproduced in soluble form, and in purified form exhibited gel electrophoretic mobilities essentially identical to that of the wild-

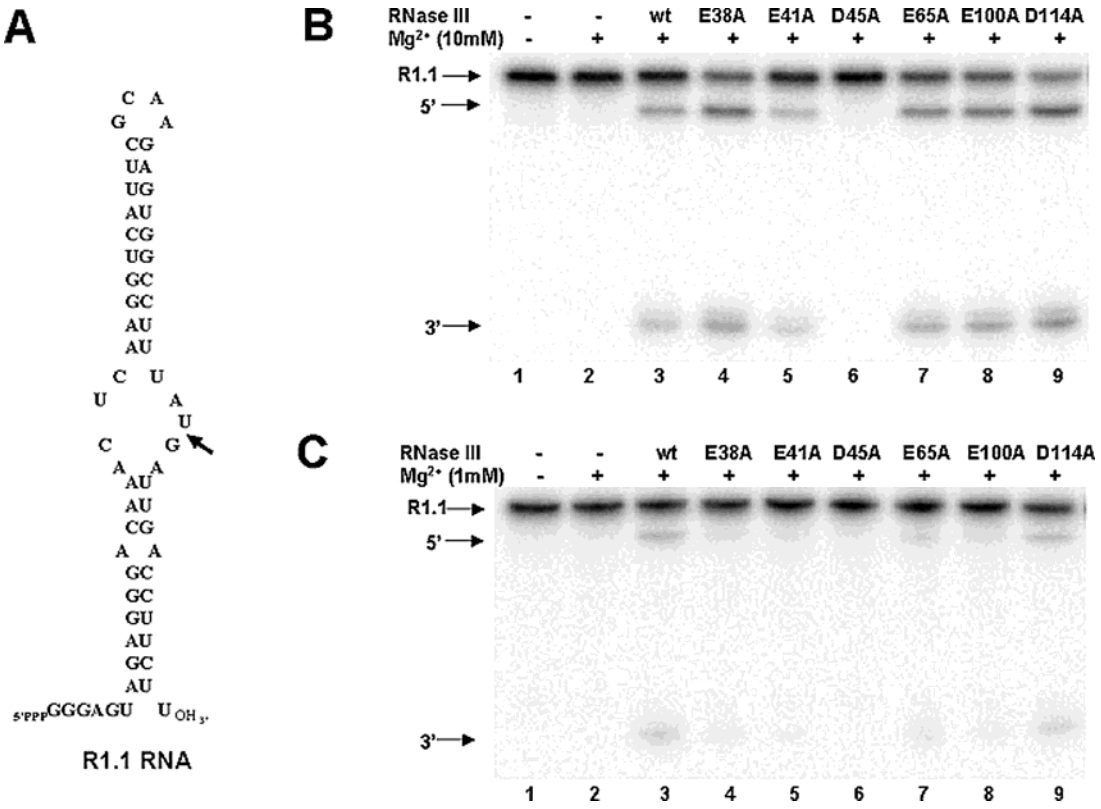

FIGURE 3: Catalytic activities of RNase III alanine mutants in the presence of 10 or 1 mM Mg^{2+}. (A) Sequence and secondary structure of R1.1 RNA (60 nt). The arrow indicates the RNase III cleavage site, the utilization of which provides two products, 47 and 13 nt in length. (B) Cleavage assays of the RNase III[E38A], -[E41A], -[D45A], -[E65A], -[E100A], and -[D114A] mutants carried out in the presence of 10 mM $MgCl_2$. Assays used internally ^{32}P-labeled R1.1 RNA and 20 nM enzyme (see Experimental Procedures). Reaction mixtures were incubated at 37 °C for 5 min before addition of Mg^{2+}, and reactions were allowed to proceed for 15 s before addition of EDTA to the mixtures (see Experimental Procedures). Reaction mixtures were electrophoresed in a 15% polyacrylamide gel and were analyzed by phosphorimaging: lane 1, R1.1 RNA (no incubation); lane 2, R1.1 RNA incubated with Mg^{2+} in the absence of RNase III; lane 3, R1.1 RNA incubated with RNase III in the absence of Mg^{2+}; and lanes 4−9, reactions using the RNase III[E38A], -[E41A], -[D45A], -[E65A], -[E100A], and -[D114A] mutants, respectively. (C) Same experiment as in panel B, except that the reaction buffer contained 1 mM $MgCl_2$.

type polypeptide (MW ~ 28 000) (data not shown). The RNase III mutants were tested for their ability to cleave a small model substrate *in vitro*. R1.1 RNA (Figure 3A) is based on the R1.1 processing signal of bacteriophage T7 (*23*). The 60 nt RNA is cleaved by RNase III at a single site within the internal loop, providing two products, 47 and 13 nt in size (*20*). Since it was possible that the two RNase III mutants could exhibit an altered dependence on divalent metal ion, the cleavage assays assessed activity at 10 and 1 mM Mg^{2+}. The 10 mM concentration is significantly higher than that needed to fully support the wild-type enzyme (~1 mM) (*4, 18*), while the 1 mM value approximates the free Mg^{2+} concentration *in vivo* (*24*). In both experiments, the monovalent salt concentration was the physiologically relevant value of 200 mM (*20*).

The RNase III[E41A] and RNase III[D114A] mutants are able to cleave R1.1 RNA in the presence of 10 mM Mg^{2+} (Figure 3B, lanes 5 and 9). The cleavage patterns are identical to that of the wild-type enzyme (Figure 3B, lane 3), indicating that the canonical cleavage site of R1.1 RNA (Figure 3A) is recognized by both RNase III mutants. A different behavior is seen at 1 mM Mg^{2+}, where the RNase III[E41A] mutant exhibits a diminished activity (Figure 3C, compare lane 5 with lane 3). The RNase III[D114A] mutant also shows diminished activity (Figure 3C, lane 9), albeit to a lesser extent in this experiment than that seen with RNase III[E41A]. A quantitative assessment of the altered Mg^{2+}-dependent behaviors was obtained by measuring the extent of substrate cleavage as a function of Mg^{2+} concentration, which allowed determination of the K^{Mg} (*12*). Table 1 gives the K^{Mg} values for the RNase III[E41A] and RNase III[D114A] mutants, which are both ~2.8-fold higher, respectively, than the K^{Mg} of the wild-type enzyme. To assess whether the E41A and D114A mutations affect other aspects of catalytic function, the steady-state kinetic parameters (K_m and k_{cat}) and catalytic efficiencies (k_{cat}/K_m) were determined at 10 mM Mg^{2+} (Table 1). Under these conditions, RNase III[D114A] is kinetically indistinguishable from the wild-type enzyme, while RNase III[E41A] exhibits a 5-fold lower k_{cat}, but a K_m only slightly different from that of RNase III. While the larger K^{Mg} suggests a reduced affinity for Mg^{2+}, the reduced k_{cat} for RNase III[E41A] indicates a catalytic defect that is not fully restored at 10 mM Mg^{2+} (see also Discussion).

The relatively modest effects of the E41A and D114A mutations were unexpected, since the *A. aeolicus* RNase III structure shows each side chain to be engaged with the bound metal ion (Figure 2) (*13*). However, the structure also reveals that an adjacency of the E41 and D114 side chains, raising the possibility that the relatively minor effects of alanine substitution may reflect the ability of each side chain to functionally compensate for the absence of the other. To examine this possibility, the RNase III[E41A/D114A] double

Table 1: Apparent K^{Mg} Values and Steady-State Kinetic Parameters of the *E. coli* RNase III[E38A], -[E41A], -[E65A], -[E100A], and -[D114A] Mutants

	WT	E38A	E41A	E65A	E100A	D114A	E41A/D114A
K^{Mg} (mM)[a]	0.46 ± 0.02	1.58 ± 0.13	1.25 ± 0.25	1.27 ± 0.08	2.48 ± 0.27	1.35 ± 0.08	39 ± 14
k_{cat} (min^{-1})[b]	8.4 ± 0.9	5.4 ± 0.9	1.9 ± 0.2	5.9 ± 0.1	43.4 ± 4.5	9.9 ± 0.1	nd[c]
K_m (nM)[b]	66 ± 11	54 ± 12	41 ± 9.5	56 ± 7	544 ± 91	71 ± 12	nd[c]
k_{cat}/K_m ($\times 10^7$ M^{-1} min^{-1}) (10 mM Mg)	13	10	4.7	11	7.9	14	−
k_{cat}/K_m(rel.) (10 mM Mg^{2+})	[1.0]	0.77	0.36	0.85	0.61	1.08	−
k_{cat}/K_m(rel.) (1 mM Mg^{2+})	[1.0]	0.17	0.05	0.16	0.11	0.52	−

[a] K^{Mg} values were determined as described in ref *12* and involved cleavage assays using 20 nM RNase III (or RNase III mutant) and internally ^{32}P-labeled R1.1 RNA (200 nM). The extent of substrate cleavage generally was within 30%. The gel electropherograms were analyzed with ImageQuant and the data subjected to least-squares curve fitting using Kaleidagraph (version 3.5). Curve fitting used the relation $Y = A[Mg]/(K^{Mg} + [Mg])$, where Y is the extent of cleavage, A the maximal extent of cleavage, and [Mg] the Mg^{2+} concentration. This relation assumes a single affinity class of metal binding sites and makes no assumption about the number of metal ions required for activity (*12*). The reported K^{Mg} values are the average of three experiments, and the standard errors of the mean are provided. [b] k_{cat} and K_m values were determined as described in Experimental Procedures, using cleavage assays involving internally ^{32}P-labeled R1.1 RNA, 20 nM RNase III (or RNase III mutant), and a buffer containing 10 mM Mg^{2+}. Nonlinear least-squares curve fitting was carried out using Kaleidagraph and applying a Michaelis−Menten kinetic scheme (*12*). The reported values are the average of three experiments, and the standard errors of the mean are also provided. [c] Not determined.

mutant was purified and its activity examined. In contrast to the single mutants, the double mutant exhibited a poor ability to cleave R1.1 RNA at 10 mM Mg^{2+} as well as at 1 mM Mg^{2+} (data not shown). The measured K^{Mg} of 39 mM for RNase III[E41A/D114A] is 85-fold higher than that of the wild-type enzyme, and also is substantially larger than would be predicted on the basis of an additive effect on K^{Mg} by the single alanine substitutions (Table 1). The behavior of the double mutant is consistent with a compensatory ability of the E41 and D114 side chains in binding metal ion (see the Discussion).

Catalytic Properties of the RNase III[E38A] and RNase III[E65A] Mutants. The *A. aeolicus* RNase III E37 and E64 side chains (corresponding to E38 and E65, respectively, of *E. coli* RNase III) are at the subunit interface (Figure 2), with the E37 side chain from one subunit within hydrogen bonding distance of the backbone amide hydrogen of residue E64 from the other subunit. However, neither side chain interacts with the bound metal (Figure 2) (*13*). It was suggested that the two side chains participate in one of the proposed dual hydrolytic mechanisms (*13*). A cleavage assay shows that RNase III[E38A] and RNase III[E65A] can cleave R1.1 RNA at 10 mM Mg^{2+} (Figure 3B, lanes 4 and 7, respectively). The catalytic efficiency of each mutant at 10 mM Mg^{2+} is comparable to that of the wild-type enzyme (Table 1). Both mutants exhibit a lower level of activity at 1 mM Mg^{2+} (Figure 3C, compare lanes 4 and 7 with lane 3), and the K^{Mg} values for RNase III[E38A] and RNase III[E65A] are 3.4- and 2.8-fold higher, respectively, than the K^{Mg} of RNase III (Table 1). We conclude that E65 and E38 are not essential for catalytic activity *in vitro*, but that substitution by alanine causes a requirement for a higher Mg^{2+} concentration for optimal activity. The implications of these behaviors with respect to potential functional roles for the E38 and E65 side chains are discussed below.

Analysis of the D45 Side Chain. Compared to the other mutations, substitution of D45 with alanine has the most severe effect on activity. Thus, RNase III[D45A] does not detectably cleave R1.1 RNA in the presence of 1 or 10 mM Mg^{2+} (Figure 3B,C, lane 6). However, the use of high enzyme concentrations (500 nM) and extended reaction times (30 min) yielded a small amount of cleavage of R1.1 RNA (data not shown). This allowed an estimation of the catalytic efficiency of RNase III[D45A], using the relationship in which the ratio of initial rates corresponds to the ratio of catalytic efficiencies (*25*). Determined in this manner, the catalytic efficiency of RNase III[D45A] (Table 2) is ~30000-fold lower than that of the wild-type enzyme. The ability of RNase III[D45A] to bind substrate was examined by a gel shift assay. To provide a comparison with the wild-type enzyme, the assay used Ca^{2+} instead of Mg^{2+} such that substrate binding could be examined in the absence of cleavage (*16*). The gel shift assay (Figure 4) reveals that RNase III[D45A] can bind R1.1 RNA in a manner comparable to that of the wild-type enzyme, with measured K'_D values of 3.9 and 4.5 nM, respectively. The retention of substrate binding ability by RNase III[D45A] is consistent with the observation that the dsRBD is the primary determinant of substrate binding (*12*).

Table 2: Steady-State Kinetic Parameters and K^{Mn} Values for RNase III[D45] Mutants

	WT	D45A	D45E	D45N
[Mg^{2+}]				
k_{cat} (min^{-1})[a]	(8.4)	nd[d]	nd[d]	(nd)[d]
K_m (nM)[a]	(66)	nd[d]	nd[d]	(nd)[d]
k_{cat}/K_m (M^{-1} min^{-1})	(1.3×10^8)	4.4×10^3	4.2×10^3	−
[Mn^{2+}]				
k_{cat} (min^{-1})[b]	(nd)[d]	0.02	0.03	0.03
K_m (nM)[b]	(nd)[d]	820	630	1100
k_{cat}/K_m ($\times 10^4$ M^{-1} min^{-1})	(nd)[d]	2.4	4.8	2.7
K^{Mn} (mM)[c]	[0.2−0.5]	25 ± 9	2.8 ± 0.5	18 ± 3

[a] Steady-state kinetic parameters were determined using internally ^{32}P-labeled R1.1 RNA, 10 mM Mg^{2+}, and an enzyme concentration of 20 nM. The extent of substrate cleavage was limited to <30%. WT enzyme kinetic constants were from Table 1. The activities of the D45A, D45E, and D45N mutants were too low to accurately determine k_{cat} or K_m. However, the catalytic efficiencies could be estimated (see the Results). [b] Kinetic constants were determined at 100 mM Mn^{2+}. The wild-type enzyme activity was negligible in the presence of 100 mM Mn^{2+}. [c] K^{Mn} values were determined as described in footnote a of Table 1. The K^{Mn} for the wild-type enzyme is an estimate, due to inhibition by Mn^{2+} at concentrations of >1 mM (see also the Results). [d] Not determined.

The behavior of RNase III[D45A] suggests that the aspartic acid is involved in an aspect of the catalytic step. RNase III[D45E] and RNase III[D45N] were examined to gain information about the side chain functional requirements. The D45E mutation allows evaluation of the importance of functional group position, while the D45N mutation allows evaluation of the requirement for an ionizable

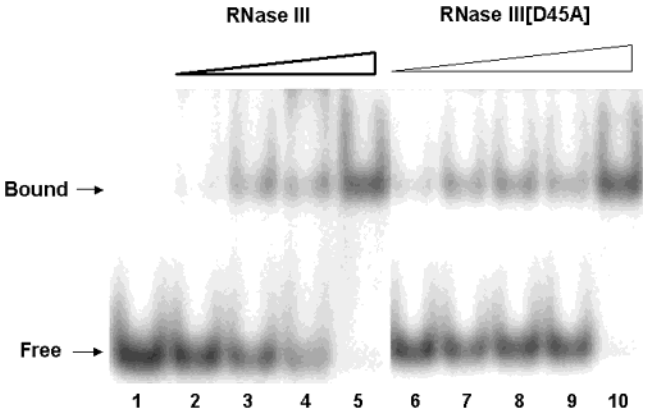

FIGURE 4: Substrate binding ability of RNase III[D45A]. The gel shift assay was performed as described in Experimental Procedures using 5′-^{32}P-labeled R1.1 RNA. The binding reaction buffer, as well as gel and electrophoresis buffers, included 5 mM $CaCl_2$. Reaction mixtures were incubated at 37 °C for 5 min, placed on ice, and then electrophoresed in a 6% polyacrylamide gel. Reactions were visualized by phosphorimaging: lane 1, no protein added; lanes 2−5, RNase III at 0.7, 1.5, 2.9, and 8.7 nM (dimer), respectively; and lanes 6−10, RNase III[D45A] mutant at 0.7, 1.4, 2.2, 2.9, and 8.6 nM, respectively. "Free" indicates the position of R1.1 RNA, while "Bound" indicates the position of the R1.1 RNA−RNase III complex.

carboxylic acid. Both mutants are defective in their ability to cleave R1.1 RNA, at either 1 or 10 mM Mg^{2+} (Figure 5A, compare lanes 4−7 with lane 3). Although the activity of RNase III[D45E] in Mg^{2+}-containing buffer was too low to accurately determine the kinetic parameters, the catalytic efficiency was able to be estimated as described above. The RNase III[D45E] catalytic efficiency (at 10 mM Mg^{2+}) is ∼30000-fold lower than that of the wild-type enzyme, and is similar to the low catalytic efficiency of RNase III[D45A] (Table 2). Gel shift assays (not shown) confirmed the retention of substrate binding affinity for each mutant, with measured K'_D values of 5.0 and 2.5 nM for RNase III[D45E] and RNase III[D45N], respectively. We conclude that the catalytic activity of *E. coli* RNase III requires a precisely positioned carboxylic acid side chain at position 45.

Mn^{2+}-Dependent Catalytic Activities of the D45 Mutants. The catalytic activity of *E. coli* RNase III is supported by Mn^{2+}, with a concentration of ∼1 mM conferring optimal activity (*4*, *12*, *18*). Since Mn^{2+} rescues the activity of RNase III[E117D] (*18*), it was worth determining whether the activities of the D45 mutants also could be rescued by Mn^{2+}. RNase III[D45A] and RNase III[D45N] cleave R1.1 RNA in the presence of either 1 or 10 mM Mn^{2+}, with the 10 mM concentration supporting a higher level of activity (Figure 5A, lanes 8−11). RNase III[D45E] cleavage of R1.1 RNA also is supported by Mn^{2+} (Figure 5A, compare lanes 5 and 9), and the Mn^{2+} concentration dependence of RNase III[D45E] activity is shown in Figure 5B. The K^{Mn} values of RNase III[D45N] and RNase III[D45A] (Table 2) are ∼60- and 80-fold larger, respectively, than the estimated K^{Mn} of ∼0.3 mM for wild-type RNase III, while the K^{Mn} for RNase III[D45E] is only 10-fold larger than that of RNase III. These data show that alteration of the D45 side chain perturbs the ability of Mn^{2+} to function as a cofactor, but with the D45E mutation having the smallest effect (see also the Discussion). Table 2 provides the K_m and k_{cat} values (determined at 100 mM Mn^{2+}) for cleavage of R1.1 RNA by RNase III[D45A], RNase III[D45E], and RNase III[D45N]. For each mutant, the k_{cat} is ∼400-fold lower and the K_m >10-fold larger than that of the wild-type enzyme (measured at 1 mM Mn^{2+}). Thus, near-saturating Mn^{2+} concentrations do not fully rescue the defective activities of the D45 mutants.

Catalytic Behavior of RNase III[E100A]. Sequence alignment (Figure 1B) reveals a glutamic acid at position 100 in all but two of the orthologs. *A. aeolicus* RNase III exhibits a six amino acid deletion in this region, while the *Mycoplasma penetrans* RNase III sequence carries an E → I change. The E100 side chain is not involved in the metal binding site, at least in the absence of substrate, and it has been noted that the *A. aeolicus* RNase III segment encompassing this position exhibits a greater degree of conformational mobility than the rest of the polypeptide (*13*). Similar to the other alanine mutants, RNase III[E100A] activity is comparable to that of wild-type enzyme at 10 mM Mg^{2+}

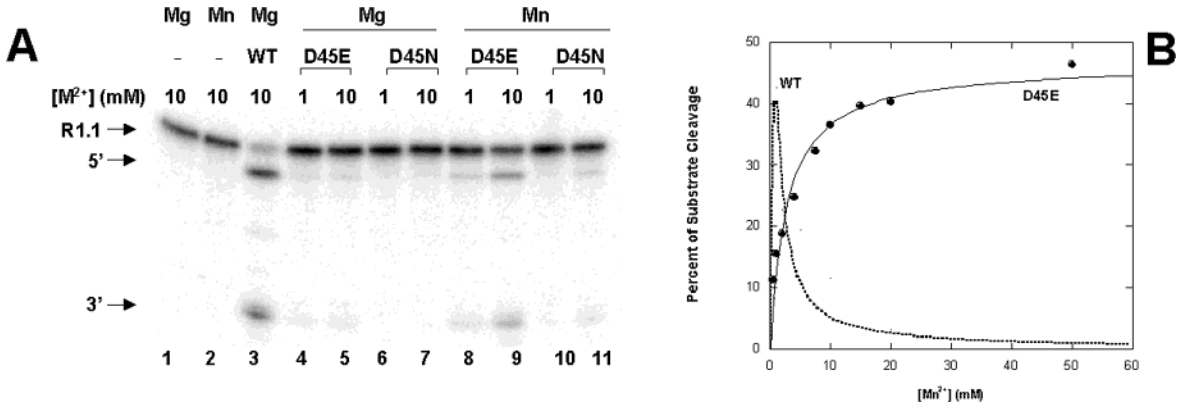

FIGURE 5: Catalytic behaviors of RNase III[D45E] and RNase III[D45N] in the presence of Mg^{2+} or Mn^{2+}. (A) R1.1 RNA cleavage reactions. Assays were performed as described in Experimental Procedures, using internally ^{32}P-labeled R1.1 RNA and an enzyme concentration of 500 nM (dimer). The buffer consisted of 30 mM Tris-HCl (pH 7.5), 200 mM NaCl, and divalent metal ion as indicated. The cleavage time was 30 min at 37 °C. Reactions were stopped with EDTA, and mixtures were electrophoresed in a 15% polyacrylamide−urea gel and analyzed by phosphorimaging (see Experimental Procedures): lane 1, R1.1 RNA incubated with 10 mM Mg^{2+} (no enzyme); lane 2, R1.1 RNA incubated with 10 mM Mn^{2+} (no enzyme); lane 3, R1.1 RNA incubated with RNase III (20 nM) in the presence of 10 mM Mg^{2+} at 37 °C for 30 s; lanes 4, 5, 8, and 9, RNase III[D45E] action on R1.1 RNA in the presence of Mg^{2+} or Mn^{2+}; and lanes 6, 7, 10, and 11, reactions involving RNase III[D45N] action on R1.1 RNA in the presence of Mg^{2+} or Mn^{2+}. (B) Mn^{2+} concentration dependence of RNase III[D45E] catalytic activity. The Mn^{2+} concentration dependence of RNase III activity is indicated by the dotted line (data taken from ref *12*). The two curves cannot be directly compared with respect to absolute activities, due to differing experimental conditions. However, the important feature is the inhibitory action of Mn^{2+} on RNase III.

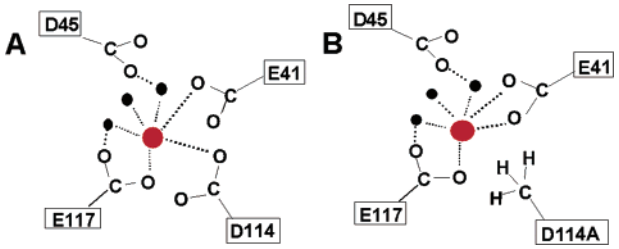

FIGURE 6: Metal ion interactions of the E41, D45, D114, and E117 side chains and potential functional redundancy of E41 and D114 side chains. (A) Interaction of acidic side chains with Mg^{2+}, also showing a probable hydrogen bond between the D45 side chain and the water-bound metal (*13*, *26*). (B) Potential functional compensation of the E41 side chain for the D114A mutation. The filled red circle represents the metal ion, and the filled black circles represent water molecules. A weakened metal ion affinity due to the D114A mutation could be compensated as shown by a monodentate to bidentate switch in metal ion coordination by the E41 side chain. A similar scenario is possible for the E41A mutation.

(Figure 3B, compare lane 8 with lane 3), but is significantly lower at 1 mM Mg^{2+} (Figure 3C, compare lane 8 with lane 3). The K^{Mg} for RNase III[E100A] is 5-fold greater than that of wild-type enzyme (Table 1), and is the largest K^{Mg} value of all the examined single alanine mutants. The steady-state kinetic parameters of RNase III[E100A] also are qualitatively distinct from the other mutants. The k_{cat} of 43.4 min^{-1} and K_m of 544 nM (10 mM Mg^{2+}) (Table 2) are 5-fold and 8-fold greater, respectively, than the corresponding values for wild-type enzyme. Thus, while the catalytic efficiency is comparable to that of wild-type enzyme, the value reflects a higher turnover rate constant coupled with an apparently weaker affinity for substrate.

DISCUSSION

This study has described the in vitro catalytic activities of *E. coli* RNase III mutants carrying alanine substitutions of conserved acidic residues within the nuclease domain. All of the mutants (with the exception of RNase III[D45A] − see below) are active in vitro and exhibit the same cleavage site specificity as wild-type enzyme. However, these mutants require distinctly higher Mg^{2+} concentrations for full activity. The crystal structure of the *A. aeolicus* RNase III nuclease domain suggests different sources of the altered metal ion dependencies. The E41 and D114 side chains of *E. coli* RNase III are expected to coordinate the Mg^{2+} ion. Changing either residue to an alanine would be expected to perturb metal binding, which is consistent with the higher K^{Mg} values, compared to that of RNase III. While the catalytic activity of RNase III[D114A] is essentially the same as wild-type enzyme at 10 mM Mg^{2+}, the apparent permanently reduced k_{cat} of RNase III[E41A] suggests that the E41 side chain may have an additional function separate from metal ion binding.

A functional redundancy of the E41 and D114 side chains is indicated by the substantially higher K^{Mg} of RNase III[E41A,D114A] compared to the K^{Mg} values of the corresponding single mutants. One scenario is that the loss of either side chain is functionally compensated by a monodentate to bidentate switch in metal coordination by the other side chain (Figure 6). Such compensation would be unavailable to the double mutant. A relaxed requirement for an aspartic acid at position 114 is suggested by the *Helicobacter pylori* RNase III sequence (Figure 1B), which contains a serine in place of aspartic acid at this position. Finally, neither the E41 nor the D114 side chain exhibits the same degree of functional importance as the E117 side chain, which engages in a bidentate interaction with metal ion (Figure 6), and whose mutation to alanine has a severe effect on activity which is not compensated by high Mg^{2+} concentrations (*16*, *18*). Direct measurement of metal ion binding affinities and structural analyses of the alanine mutants will be necessary to evaluate side chain contributions to metal binding.

The low catalytic activity of RNase III[D45A] *in vitro* (this study) and *in vivo* (*13*), along with the apparent invariance of this residue (Figure 1B), suggests an important functional role. The low activities of RNase III[D45N] and RNase III[D45E] indicate a strict requirement for a precisely positioned carboxylic acid. A function in catalysis is suggested by the proximity of the *A. aeolicus* RNase III D44 side chain to a water molecule that is coordinated to the metal ion (see Figures 2 and 6) (*13*). The dependence of the reaction rate on the metal pK_a indicates that a metal-bound hydroxide is the reaction nucleophile (*15*). It is therefore possible that the D45 side chain may serve to deprotonate the metal-bound water, creating the reactive species. Thus, RNase III[D45N] with the weakly basic aspartamide group is expected to be ineffective in this task, while the methylene shift in RNase III[D45E] could interfere with water activation by moving the carboxylic acid to a functionally suboptimal position. Finally, the low-level activity of RNase III[D45A] may reflect either activation of the water solely by metal or the involvement of an alternative protein moiety (or another water molecule).

The support of RNase III[D45E] activity by Mn^{2+} is reminiscent of the rescue of RNase III[E117D] activity by the same metal (*18*). However, the catalytic efficiency of the RNase III[D45E]−Mn^{2+} holoenzyme is ∼2700-fold lower than that of the RNase III−Mg^{2+} holoenzyme, indicating a suboptimal catalytic capacity for the former holoenzyme. Also, it is known that Mn^{2+} concentrations greater than ∼1 mM suppress RNase III activity *in vitro*, and that the E117 side chain is involved in the Mn^{2+} inhibitory site (*4*, *12*, *18*). Figure 5B suggests that RNase III[D45E] is not inhibited by Mn^{2+} and that, by inference, the D45 side chain may also be involved in the inhibitory site. However, the much lower catalytic efficiency of RNase III[D45E], coupled with a relatively high K^{Mn} value, leaves open the possibility that the Mn^{2+} inhibitory site is not affected by the D45E mutation.

RNase III[E38A] and RNase III[E65A] exhibit elevated K^{Mg} values. Since the E38 and E65 side chains do not interact with the bound metal ion (Figure 2), the cause of the altered Mg^{2+} dependence for these mutants is unclear. The two residues appear to be structurally (and perhaps functionally) interdependent, since the side chain of the *A. aeolicus* RNase III residue corresponding to E38 is hydrogen-bonded to the backbone amide hydrogen of the residue corresponding to E65 from the other subunit. It is possible that the E38 side chain stabilizes the subunit interface and perhaps also positions the E65 side chain. The *M. penetrans* RNase III ortholog contains a glutamine instead of a glutamic acid at position 38 (Figure 1B). However, as noted elsewhere (*13*), the glutamine side chain also is capable of engaging in a hydrogen bond. The retained activity of RNase III[E38A]

suggests that the proposed intersubunit hydrogen bond is dispensable, at least *in vitro*. It was reported that RNase III[E38V] is defective *in vivo* (*13*). This may reflect a requirement for a higher Mg^{2+} concentration, since the structurally similar RNase III[E38A] mutant has a 3.4-fold higher K^{Mg} than the wild-type enzyme (see also below).

It has been proposed (*13*) that the two phosphodiesters at a dsRNA target site are cleaved using separate chemistries, with each involving separate constellations of side chains. One of the proposed dual hydrolytic mechanisms involves E38 and E65, although the specific features were not presented (*13*). Our results neither support nor refute such a possibility, except that if the E38 and E65 side chains have catalytic roles, they are dispensable *in vitro*. The reported defective *in vivo* activity of RNase III[E65A] (*13*) may reflect the requirement for an increased Mg^{2+} concentration, since this mutant has an ~3-fold greater K^{Mg} than the wild-type enzyme. *Thermotoga maritima* RNase III contains a valine at the position corresponding to E65 (Figure 1B). However, a glutamic acid occupies an adjacent position, and we have shown that purified *T. maritima* RNase III can cleave R1.1 RNA *in vitro* (A. Pertzev and A. W. Nicholson, unpublished experiments).

RNase III[E100A] exhibits a steady-state kinetic behavior that is qualitatively distinct from that of the other mutants. Thus, the k_{cat} and K_m values (10 mM Mg^{2+}) are ~5- and ~9-fold greater, respectively, than those of wild-type RNase III. It is possible that weakened substrate binding, as suggested by the higher K_m, may also cause a faster rate of product release. If so, this would explain the higher k_{cat} for RNase III[E100A]. In this regard, a single-turnover kinetic analysis of *E. coli* RNase III established that the rate-limiting step occurs after the hydrolysis event (*15*). RNase III[E100A] is similar in behavior to the previously characterized RNase III[G97E] mutant, which requires a higher Mg^{2+} concentration for full activity *in vitro* (*25*). The cause of the altered Mg^{2+} dependence in this case also is unclear, but it may be related to the behavior of RNase III[E100A], since the two residues are near each other. It was noted that the segment of the *A. aeolicus* RNase III polypeptide containing E100 and G97 exhibits a significantly greater degree of structural mobility compared to the rest of the protein, and that this mobility is reduced in the presence of a divalent metal ion (*13*). Ji and co-workers have proposed that divalent metal ion stabilization of this region is important for optimal activity (*13*). However, the function of this segment in RNase III action remains to be determined.

It was also reported that the clustering of the six conserved carboxylic acid side chains creates a high negative charge density in the vicinity of the two proposed active sites (*13*). Perhaps the requirement for an increased Mg^{2+} concentration for at least some of the alanine mutants, such as E38 and E65, may represent a compensation for a general decrease in negative charge density, which in turn would weaken the overall metal binding affinity. Given a K^{Mg} of 0.46 mM, the ability of RNase III to act as an efficient catalyst *in vivo*, with an intracellular Mg^{2+} concentration of ~1 mM (*24*), may render the *in vivo* action of this enzyme sensitive to mutations that perturb metal ion affinity in an even relatively modest manner. Such mutations may include those that reduce negative charge density without altering catalytically essential side chains.

NOTE ADDED IN PROOF

Following submission of this paper, ref *27* showed that the *E. coli* RNase III[E38A] and RNase III[E65A] mutants were catalytically active in 3 mM Mg^{2+} buffer and that the RNase III[D45A] mutant exhibited negligible activity. These results are essentially in agreement with the results of our study.

ACKNOWLEDGMENT

We thank Xinhua Ji for insightful comments on this study, and Alexandre Pertzev and Wenzhao Meng for assistance with several of the experiments. We also thank Rhonda Nicholson for a critique of the manuscript, and other members of the laboratory for their advice and support.

REFERENCES

1. Nicholson, A. W. (2003) The ribonuclease superfamily: forms and functions in RNA maturation, decay, and gene silencing, in *RNAi: A Guide to Gene Silencing* (Hannon, G. J., Ed.) pp 149−174, Cold Spring Harbor Laboratory Press, Plainview, NY.
2. LaMontagne, B., Larose, S., Boulanger, J., and Abou Elela, S. (2001) The RNase III family: A conserved structure and expanding functions in eukaryotic dsRNA metabolism, *Curr. Issues Mol. Biol. 3*, 71−78.
3. Court, D. L. (1993) RNA processing and degradation by RNase III, in *Control of Messenger RNA Stability* (Belasco, J. G., and Brawerman, G., Eds.) pp 71−116, Academic Press, New York.
4. Robertson, H. D., Webster, R. E., and Zinder, N. D. (1968) Purification and properties of ribonuclease III from *Escherichia coli*, *J. Biol. Chem. 243*, 82−91.
5. Nicholson, A. W. (1999) Function, mechanism and regulation of bacterial ribonucleases, *FEMS Microbiol. Rev. 23*, 371−390.
6. Bardwell, J. C. A., Regnier, P., Chen, S. M., Nakamura, Y., Grunberg-Manago, M., and Court, D. L. (1989) Autoregulation of RNase III operon by mRNA processing, *EMBO J. 8*, 3401−3407.
7. Matsunaga, J., Simons, E. L., and Simons, R. W. (1996) *E. coli* RNase III autoregulation: structure and function of *rncO*, the posttranscriptional "operator", *RNA 2*, 1228−1240.
8. Wagner, E. G. H., and Simons, R. W. (1994) Antisense RNA control in bacteria, phages and plasmids, *Annu. Rev. Biochem. 48*, 713−742.
9. St. Johnston, D., Brown, N. H., Gall, J. G., and Jantsch, M. (1992) A conserved double-stranded RNA binding domain, *Proc. Natl. Acad. Sci. U.S.A. 89*, 10979−10983.
10. Kharrat, A., Macia, M. J., Gibson, T. J., Nilges, M., and Pastore, A. (1995) Structure of the dsRNA-binding domain of *E. coli* RNase III, *EMBO J. 14*, 3572−3584.
11. Nashimoto, H., Miura, A., Saito, H., and Uchida, H. (1985) Suppressors of temperature-sensitive mutations in a ribosomal protein gene, *rpsL* (S12), of *Escherichia coli* K12, *Mol. Gen. Genet. 199*, 381−387.
12. Sun, W., Jun E., and Nicholson, A. W. (2001) Intrinsic double-stranded-RNA processing activity of *Escherichia coli* ribonuclease III lacking the dsRNA-binding domain, *Biochemistry 40*, 14976−14984.
13. Blaszczyk, J., Tropea, J. E., Bubnenko, M., Routzahn, K. M., Waugh, D. S., Court, D. L., and Ji, X. (2001) Crystallographic and modeling studies of RNase III suggest a mechanism for double-stranded RNA cleavage, *Structure 9*, 1225−1236.
14. Dunn, J. J. (1982) Ribonuclease III, in *The Enzymes* (Boyer, P. D., Ed.) pp 485−499, Academic Press, New York.
15. Campbell, F. E., Jr., Cassano, A. G., Anderson, V. E., and Harris, M. E. (2002) Pre-steady-state and stopped-flow fluorescence analysis of *Escherichia coli* ribonuclease III. Insights into mechanism and conformational changes associated with binding and catalysis, *J. Mol. Biol. 317*, 21−40.
16. Li, H., and Nicholson, A. W. (1996) Defining the enzyme binding domain of a ribonuclease III processing signal. Ethylation interference and hydroxyl radical footprinting using catalytically inactive RNase III mutants, *EMBO J. 15*, 1421−1433.

17. Dasgupta, S., Fernandez, L., Kameyama, L., Inada, T., Nakamura, Y., Pappas, A., and Court, D. L. (1998) Genetic uncoupling of the dsRNA-binding and RNA cleavage activities of the *Escherichia coli* endoribonuclease RNase III: The effect of dsRNA binding on gene expression, *Mol. Microbiol. 28*, 629−640.
18. Sun, W., and Nicholson, A. W. (2001) Mechanism of action of *Escherichia coli* ribonuclease III. Stringent chemical requirement for the glutamic acid 117 side chain, and Mn^{2+} rescue of the Glu117Asp mutant, *Biochemistry 40*, 5102−5110.
19. He, B., Rong, M., Lyakhov, D., Gartenstein, H., Diaz, G., Castagna, R., McAllister, W. T., and Durbin, R. K. (1997) Rapid mutagenesis and purification of phage RNA polymerases, *Protein Expression Purif. 9*, 142−151.
20. Amarasinghe, A. K., Calin-Jageman, I., Harmouch, A., Sun, W., and Nicholson, A. W. (2001) *Escherichia coli* ribonuclease III: affinity purification of hexahistidine-tagged enzyme and assays for substrate binding and cleavage, *Methods Enzymol. 342*, 143−158.
21. Kindler, P., Keil, T. U., and Hofschneider, P. H. (1973) Isolation and characterization of an RNase III deficient mutant of *Escherichia coli*, *Mol. Gen. Genet. 126*, 53−69.
22. Nashimoto, H., and Uchida, H. (1985) DNA sequencing of the *Escherichia coli* ribonuclease III gene and its mutations, *Mol. Gen. Genet. 210*, 25−29.
23. Dunn, J. J., and Studier, F. W. (1983) Complete nucleotide sequence of bacteriophage T7 and the locations of T7 genetic elements, *J. Mol. Biol. 166*, 477−535.
24. Snavely, M. D. (1990) Magnesium transport in prokaryotic cells, in *Metal Ions in Biological Systems* (Sigel, H., and Sigel, A., Eds.) Vol. 26, pp 155−175, Marcel Dekker, New York.
25. Davidov, Y., Rahat, A., Flechner, I., and Pines, O. (1993) Characterization of the *rnc-97* mutation of RNAase III: a glycine to glutamate substitution increases the requirement for magnesium ions, *J. Gen. Microbiol. 139*, 717−724.
26. Blaszcyk, J., Gan, J., Tropea, J. E., Court, D. L., Waugh, D. S., and Ji, X. (2004) Noncatalytic assembly of ribonuclease III with double-stranded RNA. *Structure* (Camb.) *12*, 457−466.
27. Zhang, H., Kolb, F. A., Jaskiewicz, L., Westhof, E., and Filipowicz, W. (2004) Single processing center models for human dicer and bacterial RNase III, *Cell 118*, 57−68.

BI049258I